RSC Sustainability

ROYAL SOCIETY OF CHEMISTRY

PAPER

View Article Online
View Journal | View Issue

Cite this: *RSC Sustainability*, 2025, **3**, 3080

Recovery of valuable metals from lithium-containing aluminum electrolyte slag *via* an NaOH leaching-aging-water leaching process†

Ting Zhou,‡[a] Chenyu Zhang,‡[a] Rui Xu,[ab] Sha Luo,*[a] Wenzhang Li [a] and Yang Liu *[a]

With the continuous development of aluminum electrolysis technology, a large amount of lithium–aluminum electrolyte is stacked as waste. In this study, a "sodium hydroxide leaching-aging-water leaching" process was employed for the resource recovery of lithium, aluminum, and fluoride from this hazardous waste. The leaching efficiency of Li achieved 90.1% under the following conditions: NaOH concentration of 10 mol L^{-1}, reaction temperature of 90 °C, reaction time of 4 hours, and liquid–solid ratio of 9 : 1. An analysis of the degree of influence of reaction factors on the leaching efficiencies of valuable metals using the orthogonal design method indicated the following relationship: NaOH concentration > liquid–solid ratio > reaction temperature > reaction time. Owing to the common ion effect, fluoride was precipitated in the form of NaF, and an NaF product with a purity of 99.6% was obtained. After aging the leaching filtrate, $LiAl_2(OH)_7{\cdot}xH_2O$ was obtained, and ~100% lithium was extracted by water leaching at 200 °C within a reaction time of 6 hours. The residue was an AlOOH product with a purity of 99.3%, and Li_2CO_3 was obtained *via* carbonation. This process provides a strategy for resource recycling and alleviating environmental crises.

Received 24th March 2025
Accepted 15th May 2025

DOI: 10.1039/d5su00210a

rsc.li/rscsus

Sustainability spotlight

A large amount of lithium–aluminum electrolyte is discharged as waste residue from aluminum electrolysis factories. This study provides a strategy to recover lithium, fluoride and aluminum using a sodium hydroxide leaching-aging-water leaching process. Moreover, this work aligns with the UN sustainable development goal SDG-12: ensure sustainable consumption and production patterns.

1. Introduction

Aluminum electrolysis technology is continuously developing, and the electrolyte always contains high contents of Li and K. Excessive LiF in the electrolyte may lead to reduced solubility of alumina, and an excessive amount of KF may lead to decreased molten salt conductivity.[1] In addition, it accelerates precipitation in the electrolytic cell, thereby reducing the lifespan of cells.[2,3] According to the literature,[4–6] aluminum electrolysis industries in China generate approximately 250 000 tons of solid waste annually, with the cumulative storage exceeding 2 million tons to date. Thus, a large amount of lithium–aluminum electrolyte is discharged in the form of waste residue, which contains cryolite (Na_3AlF_6), lithium cryolite (Na_2LiAlF_6), potassium cryolite (K_2NaAlF_6), and fluorite (CaF_2).[7] Generally, these wastes are resorted to open-air storage or landfill disposal.[8,9] However, these disposal methods need large areas of land and pose the risks of pollution owing to the chance of dissolution of fluoride into the surrounding soil and water. In particular, soluble fluorides may alter soil structure and cause biological "fluorosis".[10,11] Therefore, waste aluminum electrolyte slag is classified as hazardous waste and is listed in the "National Catalogue of Hazardous Wastes" and the European Waste List. Proper and rational waste treatment has become a major focus of the industry.[8] Although waste aluminum electrolyte slag is unsuitable for reuse in the aluminum smelting industry, it represents a high-quality source of lithium, fluoride, and aluminum resources.[12,13] Recently, the recycling of Li and other valuable elements from waste has gained

[a]*School of Chemistry and Chemical Engineering, Central South University, Changsha, 410083, China. E-mail: rosa619@qq.com; yangliu_csu@csu.edu.cn*

[b]*Xuzhou China Mining Geotechnical Technology Co., Ltd, China*

† Electronic supplementary information (ESI) available: Table for main element content of material; XRD pattern of aluminum electrolyte slag; SEM images, EDS data; leaching efficiency of valuable metals under the conditions of 4.44 mol per L NaOH, 90 °C, L/S = 9; factorial design experimental conditions and leaching efficiency of response variables; mass fractions of Li and Al in Li/Al-LDHs sample; mass of main product; consumption in different methods for recovery lithium into Li_2CO_3 (1 kg) from the lithium-containing slags; and estimated input cost and output value in this method. See DOI: https://doi.org/10.1039/d5su00210a

‡ The authors contribute equally for this work.

increasing attention from numerous researchers.[14–19] Therefore, the scientific and standardized utilization of lithium-containing aluminum electrolyte slag holds significant economic and environmental importance for resource utilization and detoxification of aluminum smelting slag.[20–22]

To achieve the target, a hydrometallurgical process was considered, and acid leaching methods were primarily used for pre-treatment.[23–25] Wang *et al.* utilized 6% sulfuric acid for leaching lithium-containing aluminum electrolyte slag, resulting in a leachate containing Li_2SO_4.[26] Subsequent pH adjustment and purification were performed by adding NaOH and EDTA, followed by an alkali decomposition reaction with Na_2CO_3 to yield the Li_2CO_3 product. Hou *et al.* reported a leaching method using HNO_3 with Na_3AlF_6 and $LiNO_3$ as the resulting products.[27] In addition to acid leaching, aluminum salts were added as leaching agents. Wu *et al.* used HNO_3 + $Al(NO_3)_3$, and Li_2CO_3 and $Al_2((OH)_{0.46}F_{0.54})_6(H_2O)$ were obtained as products.[28] Recently, Cui *et al.* used an $AlCl_3$ + HCl solution as the leaching agent, and 88.3% of the Li^+ was leached out using 0.85 M of $AlCl_3$ with an S/L ratio of 1 : 3 at a leaching temperature of 95 °C and pH of 0.5.[29]

At the same time, roasting was also discussed by several research groups. Dong *et al.*[30] and Tang *et al.*[31] both employed a sulfuric acid roasting method to induce the phase transformation of the lithium-containing phase in the aluminum electrolyte slag at high temperatures, converting it into soluble $NaLiSO_4$. The former obtained a 98.6% purity Li_2CO_3 product by water leaching, impurity removal, and lithium precipitation process. After roasting and water leaching, Tang *et al.* separated Al^{3+} from Li-containing leachate using sodium benzoate and recovered LiF and $Al_2(SO_4)_3$ as products.[31] Wu *et al.* reported a roasting and two-stage leaching process for extracting lithium and potassium by forming water-insoluble $LiAlO_2$ and water-soluble $KAlO_2$.[32] Zhang *et al.* reported calcium salt roasting and reported that 97% of lithium can be leached using water leaching.[33] Additionally, Cai *et al.* employed a water vapor atmosphere to roast aluminum electrolyte slag for defluorination, achieving a defluorination rate of 93% when the material was heated at 950 °C for 3 hours with an inert gas flow rate of 3.5 g min^{-1}.[34] The maximum roasting temperature for this method can reach 1100 °C, but high-temperature equipment is necessary. Recently, Yang *et al.* noted a leaching transformation followed by the purification of fluorine and separation of aluminum, and they reported that fluorine and aluminum were recovered into CaF_2 and $Al(NO_3)_3$.[35]

Based on the aforementioned analysis, acid leaching achieved high extraction rates for elements, albeit with limited selectivity.[36] This method requires an extensive process for element separation and consumes a significant number of neutralizing agents, which poses challenges for waste treatment. Roasting is a streamlined process that does not involve complex chemical reactions but is associated with high energy costs.[37] The purity of the recovered products is also susceptible to the temperature and atmosphere used during roasting, which necessitates subsequent processing.

In this study, sodium hydroxide was chosen as the leaching agent for aluminum electrolyte slag. The "alkaline leaching-aging-water leaching" method was employed for lithium extraction, with fluorine being recovered in the form of NaF. Single-factor experiments were conducted to investigate the impact of NaOH concentration, reaction temperature, reaction time, and liquid–solid ratio on the leaching rates of various valuable metals. Furthermore, a factorial design method was used to establish regression models for various metals, exploring the interactions among different factors and determining the extent of their influence on metal ion leaching rates. Finally, the solid-phase aging of the leachates was further treated by water leaching followed by filtration, and Li_2CO_3 and AlOOH were obtained as products to achieve the separation of Li and Al.

2. Experiment

2.1 Materials

In this study, the aluminum electrolyte slag was provided by a company in Zhuhai (Fig. 1a). The slag was crushed in a ball mill and sieved (sieve aperture 0.1 mm) to obtain the undersized material, as shown in Fig. 1b. The lithium–aluminum electrolyte slag exhibits complex properties, with XRF analysis revealing the major elemental contents (wt%), including F, Na, Al, Ca, and K (Table S1†). ICP analysis indicated a lithium content of 1.07 wt%. XRD analysis (Fig. S1†) indicates that the aluminum electrolyte slag may contain Na_3AlF_6, $LiNa_2AlF_6$, K_2NaAlF_6, and CaF_2. Among these, cryolite (Na_3AlF_6) is the main component in Hall–Héroult aluminum electrolysis, and alumina additives and impurities introduce lithium, potassium, and calcium into the electrolyte, forming $LiNa_2AlF_6$, K_2NaAlF_6, and CaF_2. Fig. S2† shows SEM images of the aluminum electrolyte slag, which contains particles with relatively smooth surfaces, and the size is around 20 μm. Fig. S3† presents the elements in four regions of the SEM images, and the elements are consistent with the XRD results.

2.2 Experimental procedure

The process is shown in Fig. 2, which involves leaching aluminum electrolyte slag with NaOH solution, aging Li/Al-LDHs from NaOH leaching filtrate, and leaching Li/Al-LDHs with water.

2.2.1 Sodium hydroxide leaching experiment. To investigate the effect of leaching conditions, NaOH was dissolved in deionized water to prepare leaching media with different concentrations (1.1–10 mol L^{-1}). The aluminum electrolyte powder was leached in NaOH solution at 30–150 °C for 10–240 min, with a liquid-to-solid ratio ranging from 3–18 : 1 mL g^{-1}. After the leaching process, the mixture was rapidly cooled to

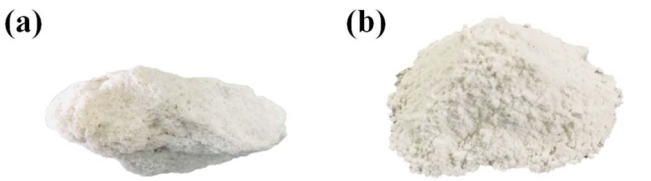

Fig. 1 (a) Aluminum electrolyte slag (a) before and (b) after crushing and sieving in a ball mill.

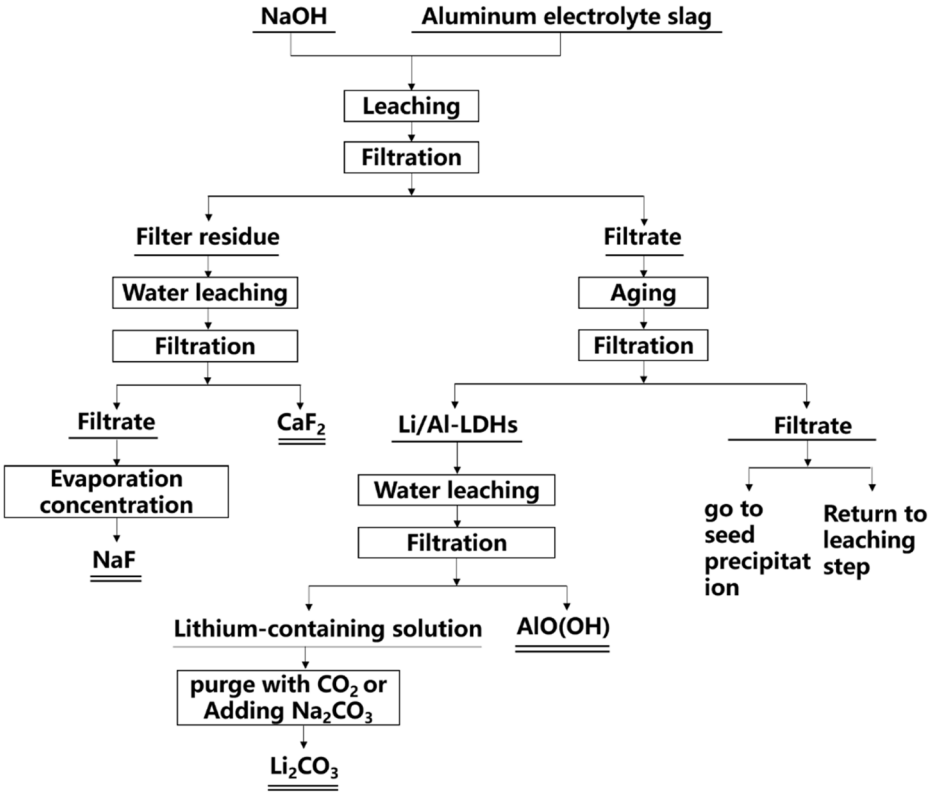

Fig. 2 Process technology roadmap.

room temperature by physical cooling, followed by filtration. The leaching efficiency can be calculated according to formula (1):

$$R = m_L/m_r \times 100\% \quad (1)$$

where R is the leaching efficiency of the element; m_L is the mass (g) of the element in the leachate; and m_r is the mass (g) of the element in the powder sample.

2.2.2 Aging Li/Al-LDHs from NaOH leaching filtrate. NaOH leachates under various reaction conditions were subjected to aging at room temperature for 3 days. After aging, filtration was performed to achieve solid–liquid separation, and the solid was dried and weighed. A 1 mL aliquot of the liquid phase was collected and diluted for ICP-OES analysis to determine the metal content.

2.2.3 Li/Al-LDHs water leaching. To further separate Li from Li/Al-LDHs, deionized water was used as the leaching agent. The leaching efficiency of Li was investigated at temperatures ranging from 40 °C to 200 °C. The optimal reaction temperature was determined based on the experimental conditions, and the reaction time was extended at this temperature to calculate the leaching efficiency of Li.

2.3 Characterization

The crystal phase of the raw material, solid residues, and products was determined by X-ray diffraction (XRD, D/max 2550VB, D8 Advance). The elemental contents were confirmed by X-ray fluorescence spectroscopy (XRF, Shimadzu XRF-1800) and inductively coupled plasma emission spectrometry (ICP, PerkinElmer Avio 500). For the ICP measurements, an aqua regia solution was used to dissolve the solid sample, which was further diluted before the test.

3. Results and discussion

3.1 Thermodynamic analysis

In the process of leaching lithium-containing aluminum electrolyte slag with sodium hydroxide solution, the reaction

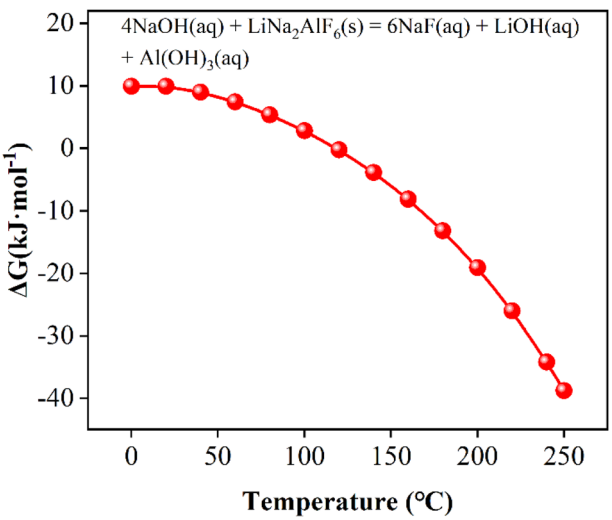

Fig. 3 Gibbs free energy (ΔG) at different temperatures (T) for the reaction between NaOH and $LiNa_2AlF_6$.

described in eqn (2) may occur. The Gibbs free energy (ΔG^{Θ}) in the range of 0–250 °C was calculated using HSC software as a function of temperature (T), as shown in Fig. 3. ΔG decreases gradually with increasing temperature. The ΔG can be smaller than 0 at low temperature and may also work if the NaOH concentration is sufficiently high.

$$4NaOH(aq) + LiNa_2AlF_6(s) \rightarrow 5NaF(aq) + LiOH(aq) + Al(OH)_3(aq) \quad (2)$$

3.2 Effects of the leaching conditions on the NaOH leaching process

Under the conditions of a reaction temperature of 90 °C, a liquid (NaOH solution)-to-solid (lithium containing aluminum electrolyte slag) ratio of 9 : 1, and a reaction time of 4 hours, the influence of different NaOH solution concentrations on the leaching rates of various valuable metals was investigated. As shown in Fig. 4a, the leaching efficiency of Li continuously increased with increasing NaOH concentration, whereas the leaching efficiency of Al and K increased at NaOH concentrations of 1.1–4 and 1.1–2, respectively. At a concentration of 5.6 mol L^{-1}, the leaching efficiencies of Al, Li, and K were 92.1%, 67.6% and 55.7%, respectively. When the sodium hydroxide concentration reaches 10 mol L^{-1}, the leaching efficiency of Li reaches 90.1%, whereas that of Al and K are ~100% and 64.8%, respectively.

To investigate the influence of reaction temperature on the leaching efficiencies of various valuable metal elements, leaching was performed under the conditions of a liquid–solid ratio of 9 : 1, NaOH concentration of 5.6 mol L^{-1}, and reaction time of 4 hours. In Fig. 4b, the leaching efficiencies of Al, Li and K gradually increase with the reaction temperature, and the leaching efficiency of Al increases slowly if the temperature is higher than 90 °C. The leaching efficiency of Li reached 79.1% at 120 °C, while the leaching efficiency of K did not change much.

The leaching efficiencies of valuable metals as a function of liquid–solid ratios were also explored under the conditions of a NaOH solution concentration of 5.6 mol L^{-1}, reaction temperature of 90 °C, and reaction time of 4 hours. In Fig. 4c, the leaching efficiencies of Al and Li increase with increasing liquid–solid ratio, whereas the leaching efficiency of K remains at ~55%. Considering the leaching efficiency, a liquid–solid ratio of 9 : 1 (mg L^{-1}) is a more suitable choice.

To investigate the effects of reaction time on the leaching efficiency of each valuable metal in the aluminum electrolyte slag, experiments were conducted under the conditions of 4.44 mol per L NaOH, 90 °C, L/S = 9 (Fig. S4†) and 5.56 mol per L NaOH, 75 °C, L/S = 9 (Fig. 4d), respectively. With the extension of the reaction time, the leaching efficiency of Al, Li and K continuously increased and reached a stable state within 1 h.

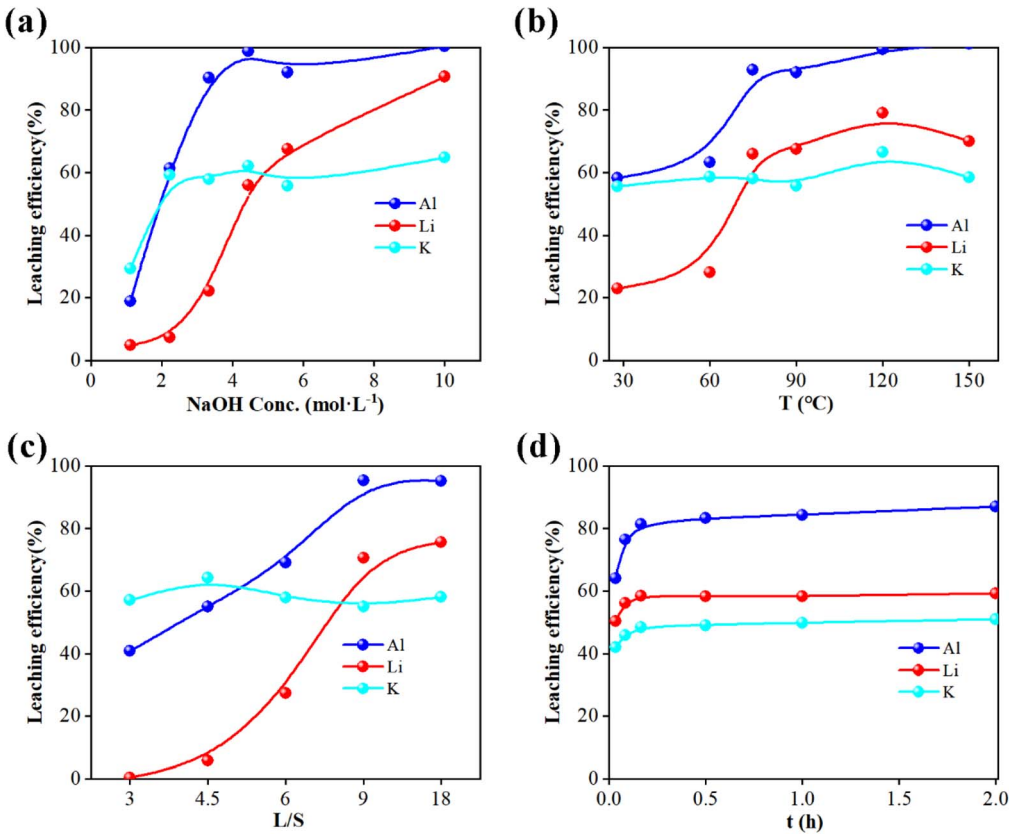

Fig. 4 Effect of (a) NaOH concentration, (b) reaction temperature, (c) liquid–solid ratio and (d) reaction time on the leaching efficiency of valuable metals.

Based on the above results, the optimal leaching conditions for the single-factor experiments of the lithium-containing aluminum electrolyte slag and NaOH leaching system were as follows: NaOH solution concentration of 10 mol L^{-1}, reaction temperature of 200 °C, reaction time of 4 hours, and liquid–solid ratio of 9 : 1. Under these conditions, the leaching rates of Al, Li, K, and Ca were 80%, 90.1%, 85.1%, and close to 0%, respectively.

3.3 Factorial design and regression equations

Based on the above experimental results, a factorial design method from the Design of Experiments (DOE) was employed to further explore the interactions between individual factors[38,39] and determine key influencing factors.[40] According to the experimental factorial design (Table S2†), the regression models for the leaching efficiencies of Al, Li, K and Ca are expressed by eqn (3)–(5), respectively.

$$\mathrm{Al}\ (\%) = -0.941 - 0.175x_3 + 0.012x_1 + 0.083x_2 - 0.014{x_3}^2 - 0.031{x_1}^2 - 0.030{x_2}^2 + 34.221x_1x_2x_3x_4 \quad (3)$$

$$\mathrm{Li}\ (\%) = -0.48x_1 - 6.65x_2 - 25.79x_3 + 1.04x_4 - 20.16{x_1}^2 + 1.68{x_2}^2 - 6.68{x_4}^2 - 8.15x_1x_2 - 1.06{x_4}^3 \quad (4)$$

$$\mathrm{K}\ (\%) = 0.594 + 0.008x_1 - 0.033x_2 - 0.067x_3 + 0.009x_4 - 0.004{x_2}^2 - 0.019{x_3}^2 - 0.012x_3x_4 + 0.003{x_2}^3 + 0.013{x_3}^3 \quad (5)$$

Based on the significance analysis of the factors and responses in the regression models for the four metal ions (Tables S3–S5†), the relationships between various factors and the leaching efficiency of the metal ions were established. In pursuit of enhancing the leaching efficiency of Li and Al, the NaOH concentration exerts the greatest influence on the leaching efficiency of both metals, and the hierarchy of influence among the four factors is established as follows: NaOH concentration > liquid-to-solid ratio > reaction temperature > reaction time. Thus, the NaOH concentration and the liquid-to-solid ratio are two key factors that need to be considered in this method.

3.4 Crystallization of leachate by aging

The leachates obtained in the above experiments were stacked at room temperature. After 7 days, precipitation was notably observed. To study the changes in ion concentration in the solution after aging, the supernatant of the aged samples was tested, as shown in Fig. 5. The concentration of Li is lower than 0.015 g L^{-1}, which is about 0.1–0.8 g L^{-1} in the raw leaching solution. In other words, lithium is almost always retained in the precipitate. Moreover, the precipitate was removed and measured by XRD (Fig. 6), whose diffraction peaks match the standard card PDF #31-0704 for $LiAl_2(OH)_7 \cdot xH_2O$. In Fig. S5 and S6,† the SEM image presents agglomerated flakes with small amounts of impurities, and the size of the particle is about 24 μm. In the ICP results of the precipitate (Table S6†), the molar ratio of Al to Li was 1.9, closely resembling the ratio in the $LiAl_2(OH)_7 \cdot xH_2O$ molecule. $LiAl_2(OH)_7 \cdot xH_2O$ is a layered

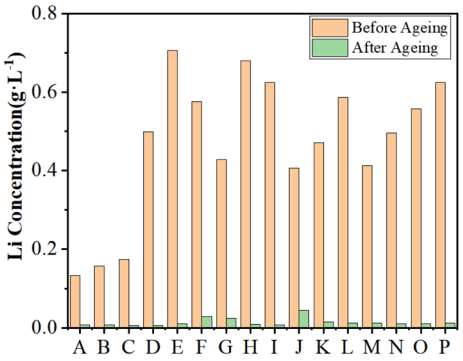

Fig. 5 Concentrations of Li before and after aging of the leaching solution obtained in different experiments.

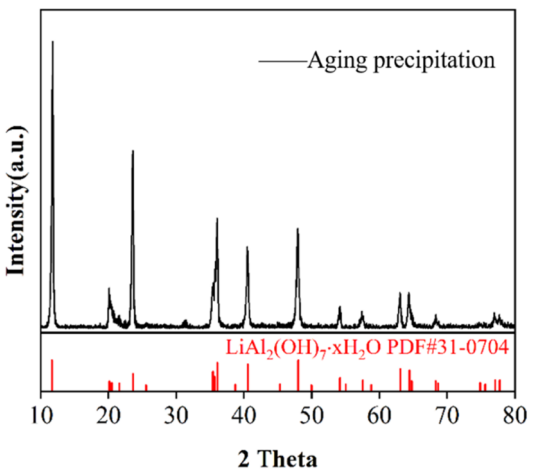

Fig. 6 XRD pattern of the filter residue of the aging solution after the primary leaching method.

crystalline compound similar to hydrotalcite, which can be represented by Li/Al-LDHs.[41,42] It consists of octahedral layers and O-coordination stacking, with hydroxyl groups located at the six vertices of the octahedral structure and water molecules inserted between the layers.[43] In each layer, only two-thirds of the cavities formed by O are occupied by Al^{3+}, leaving a remaining cavity radius of approximately 0.7 Å (1 Å = 0.1 nm), while the radius of Li^+ is about 0.68 Å, enabling it to penetrate the interlayer cavities.[44] Thus, in this step, Li is separated from K and Na.

3.5 Exploration of lithium extraction from Li/Al-LDHs

To achieve the separation of Li and Al from Li/Al-LDHs, a water leaching method was employed, thereby obtaining high-purity aluminum products and a lithium-containing solution.

The leaching efficiency of Li was investigated at a reaction time of 4 hours and a liquid-to-solid ratio of 100 : 1, with the influence of different reaction temperatures (40–200 °C), as depicted in Fig. 7a. As the reaction temperature rises, the leaching efficiency of Li steadily increases, whereas the leaching efficiency of Al remains stable at around 20%, showing no significant variation with temperature. At a reaction

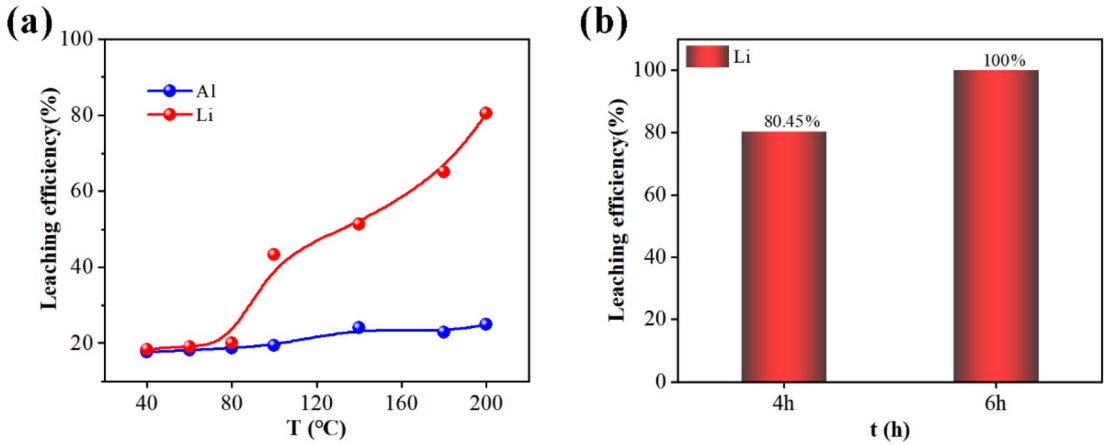

Fig. 7 (a) Leaching efficiencies of Li and Al in water leaching reaction at different temperatures. (b) Leaching efficiencies of Li with reaction time of 4 h and 6 h.

temperature of 200 °C, the leaching efficiency of Li reached 80.45%, identifying 200 °C as the optimal reaction temperature. The leaching time was further extended to 6 h, and the leaching efficiency of Li achieved ~100% (Fig. 7b).

Subsequently, lithium carbonate products were obtained after the precipitation of lithium carbide, and their XRD spectrum is shown in Fig. 8a. The SEM image shows that Li_2CO_3 is a crystalline particle with a smooth surface and a size of ~30 μm (Fig. S7†). The residue from solid–liquid separation by water leaching was analysed by XRD, as shown in Fig. 8b. The diffraction peaks correspond to the standard card PDF #83-2384 for AlO(OH), indicating the formation of boehmite after Li

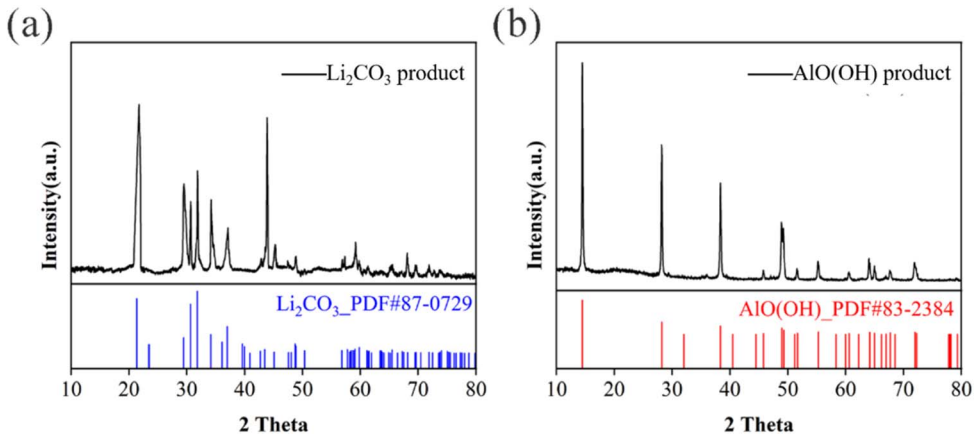

Fig. 8 (a) Carbonized lithium precipitation filter slag. (b) XRD pattern of the filter residue after leaching Li/Al-LDHs using water.

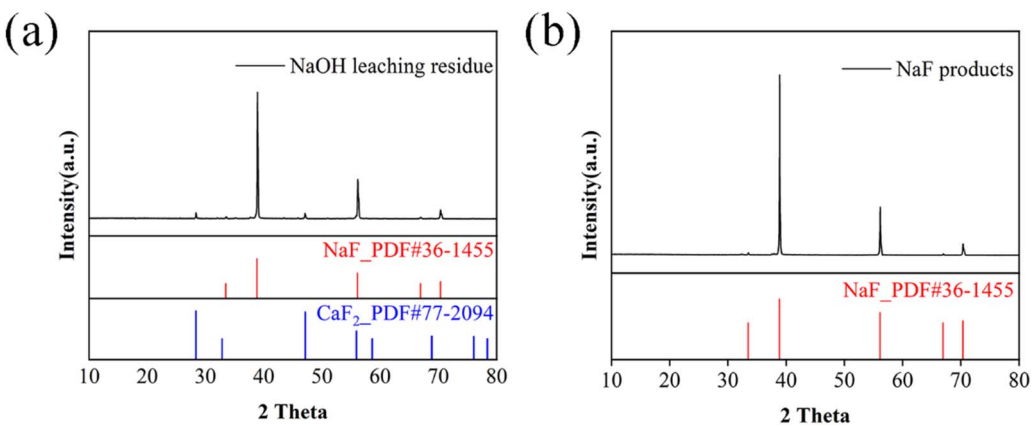

Fig. 9 XRD patterns of (a) the filter residue after leaching with sodium hydroxide and (b) NaF product.

leaching. The SEM image of AlOOH (Fig. S8†) presents agglomerated flakes, which look like LiAl-LDH in Fig. S5.† The main elements detected by EDS were Al and O (Fig. S9†).

3.6 Preparation of the NaF product

The highest concentration of NaOH used in the experiment is 10 mol L^{-1}, which is equivalent to a Na^+ concentration of 230 g L^{-1}. According to the research by Wang *et al.*[45] at this Na^+ concentration, the solubility of NaF decreases from approximately 43 g L^{-1} in water to approximately 5 g L^{-1} at 30 °C. Consequently, the primary phases of the NaOH leaching residue are NaF and CaF_2 (Fig. 9a). Based on the solubility differences between CaF_2 and NaF, a water washing method was employed to dissolve soluble NaF, followed by evaporation and crystallization to obtain the NaF product. The XRD pattern of the product is shown in Fig. 9b. The ICP analysis of the dissolved sample revealed a purity of 99.6%. The SEM image (Fig. S10†) shows a relatively flat surface of NaF (~24 μm), and limited impurity elements remaining in the NaF. The yield of NaF is about 82% (without considering the loss due to overflow and residual in the breaker during evaporation), and the consumption for synthesizing Li_2CO_3 is compared with that of reported methods (Fig. S11 and Table S7†). In summary, the output value (~359.87 RMB for 45.48 kg NaF and 1 kg Li_2CO_3) was larger than the input cost (~82.83 RMB) in this method (Table S8†).

4. Conclusion

In this study, an alkaline leaching-aging-water leaching method was employed to extract lithium from aluminum electrolytic slag, and sodium hydroxide was used as the leaching agent. The NaOH concentration and liquid–solid ratio had a more significant effect on leaching than the reaction temperature and time. The leaching efficiencies of Al, Li and K were ~100%, 90.1%, and 64.8%, respectively. Fluorine was recovered in the form of NaF due to its decreasing solubility in NaOH solution. Furthermore, $LiAl_2(OH)_7 \cdot xH_2O$ was obtained after aging the leaching filtrate, which helped in the separation of Li from K. Finally, aluminum and lithium were recovered in the form of AlOOH and Li_2CO_3 after water leaching and carbonation. This study provides a method for recovering valuable metal from aluminum electrolytic slag, which may also be useful for recovering other waste products containing lithium and aluminum.

Data availability

Data for this article, including [.opju], are available at [Baidu Netdisk] at [**https://pan.baidu.com/s/12P9PYZrfvMHlta9CCWJ6rw**].

Conflicts of interest

The authors declare that they have no known competing financial interests or personal relationships that could have appeared to influence the work reported in this paper.

Acknowledgements

This study was supported by the Joint Funds of the National Natural Science Foundation of China (no. U22A20170) and the Hunan Provincial Natural Science Foundation of China (no. 2020JJ5693). The aluminum electrolyte slag was provided by Zhuhai Ruifeimente Technology Co. Ltd.

References

1 B. Chen, J. Peng, Y. Wang and Y. Di, *Trans. Nonferrous Met. Soc. China*, 2022, **32**, 2727–2735.
2 A. Gil and S. A. Korili, *Chem. Eng. J.*, 2016, **289**, 74–84.
3 S. X. Huan, Y. W. Wang, J. P. Peng, Y. Z. Di, B. Li and L. D. Zhang, *Miner. Eng.*, 2020, **154**, 106386.
4 L. M. Dong, F. Jiao, W. Liu, S. Y. Gu, C. Wang and W. Q. Qin, *J. Cleaner Prod.*, 2023, **429**, 139326.
5 Y. M. Wang, X. X. Wang and M. Bilal, *Front. Chem.*, 2022, **10**, 1025990.
6 S. Y. Hu, D. Y. Wang, D. Hou, W. Zhao, X. L. Li, T. P. Qu and Q. D. Zhu, *Materials*, 2021, **14**, 5855.
7 S. Wu, W. Tao, Y. Zheng, H. Ge, J. He, Y. Yang and Z. Wang, *Waste Manage.*, 2021, **134**, 89–99.
8 X. K. Li, Y. Liu and T. A. Zhang, *Waste Manage. Res.*, 2023, **41**, 1498–1511.
9 L. T. Ma, Z. S. Qiu, Y. S. Tang, W. Z. Yang, B. S. Chen, J. Jiang and Y. Lin, *Environ. Chem. Lett.*, 2024, **22**, 2531–2552.
10 Q. Huo, R. Y. Li, M. Y. Chen, R. Y. Zhou, B. Li, C. Q. Chen, X. Liu, Z. Q. Xiao, G. Z. Qin, J. H. Huang and T. F. Long, *J. Hazard. Mater.*, 2024, **469**, 133838.
11 J. L. Han, L. Kiss, H. B. Mei, A. M. Remete, M. Ponikvar-Svet, D. M. Sedgwick, R. Roman, S. Fustero, H. Moriwaki and V. A. Soloshonok, *Chem. Rev.*, 2021, **121**, 4678–4742.
12 A. V. Olivares, E. Pastor-Vallés, J. B. Pettersen and G. Tranell, *Waste Manage.*, 2024, **182**, 11–20.
13 R. Xu, S. Luo, W. Z. Li, C. Y. Zhang, Z. H. Chen, Y. Wang, Y. Liu and J. Li, *Ind. Eng. Chem. Res.*, 2023, **62**, 14537–14547.
14 M. Bhar, S. Ghosh, S. Krishnamurthy, Y. Kaliprasad and S. K. Martha, *RSC Sustainability*, 2023, **1**, 1150–1167.
15 K. Davis and G. P. Demopoulos, *RSC Sustainability*, 2023, **1**, 1932–1951.
16 S. Gulliani, M. Volpe, A. Messineo and R. Volpe, *RSC Sustainability*, 2023, **1**, 1085–1108.
17 C. Liu, Y. Cao, W. Sun, T. Zhang, H. Wu, Q. Liu, Z. Rao and Y. Gu, *RSC Sustainability*, 2023, **1**, 270–281.
18 P. Thissen, A. Bogner and F. Dehn, *RSC Sustainability*, 2024, **2**, 2092–2124.
19 G. Zante, C. E. Elgar, J. M. Hartley, R. Mukherjee, J. Kettle, L. E. Horsfall, A. Walton, G. D. J. Harper and A. P. Abbott, *RSC Sustainability*, 2024, **2**, 320–347.
20 C. Z. Ren, S. Wu, W. L. Wang, L. Chen, Y. H. Bai, T. T. Zhang, H. Li and Y. X. Zhao, *J. Build. Eng.*, 2023, **64**, 105550.
21 R. Kikuchi, *Resour., Conserv. Recycl.*, 2001, **31**, 137–147.
22 A. Gil, S. Albeniz and S. A. Korili, *Chem. Eng. J.*, 2014, **251**, 43–50.
23 H. Peng, J. Guo, L. P. Lv, H. S. Huang and B. Li, *Environ. Chem. Lett.*, 2021, **19**, 1383–1393.

24 W. Liu, M. Liu, F. Ma, M. Qin, W. Zhong, X. Chen, Z. Zeng, S. Cheng and J. Xie, *Sci. Bull.*, 2024, **69**, 1697–1705.
25 C. L. Yue, H. M. Sun, W. J. Liu, B. B. Guan, X. D. Deng, X. Zhang and P. Yang, *Angew. Chem., Int. Ed.*, 2017, **56**, 9331–9335.
26 W. Wang, W. J. Chen and H. T. College, *Hydrometallurgy*, 2019, **185**, 88–92.
27 J.-f. Hou, Z.-w. Wang, T.-f. Li, Z.-n. Shi and X.-w. Hu, in *Light Metals 2016*, ed. E. Williams, Springer International Publishing, Cham, 2016, pp. 353–357, DOI: **10.1007/978-3-319-48251-4_58**.
28 S. H. Wu, W. J. Tao, Y. C. Zheng, Y. J. Yang, J. Y. Yu, J. B. Cui, Y. Lu, Z. N. Shi and Z. W. Wang, *Hydrometallurgy*, 2020, **198**, 105505.
29 L. Cui, W. Wang, X. Chao, J. Gao and F. Cheng, *J. Cleaner Prod.*, 2024, **439**, 140800.
30 L. Dong, F. Jiao, W. Liu, D. Wang, W. Chen and W. Qin, *J. Environ. Manage.*, 2024, **359**, 120963.
31 C. Tang, J. Wang, S. Yang, X. Zhang, S. Li, Y. Lai, Z. Tian, S. Jin and Y. Chen, *Resour., Conserv. Recycl.*, 2023, **197**, 107070.
32 S. Wu, W. Tao, H. Ge, J. Yang, J. Li, J. He, Y. Yang and Z. Wang, *Environ. Sci. Pollut. Res.*, 2024, **31**, 44348–44360.
33 T. Zhang, F. Liu, H. Chen, Z. Chen, C. Liao, F. Chen and Y. Guo, *ACS Sustain. Chem. Eng.*, 2024, **12**, 11797–11808.
34 W. C. Cai, H. Y. Xia, Q. Zhang, G. Y. Jiang and Y. J. Xu, *Jom*, 2023, **75**, 400–406.
35 J. Yang, W. Tao, J. Li, L. Kong, S. Wu, J. He, Z. Liu, Y. Sun and Z. Wang, *Sep. Purif. Technol.*, 2025, **357**, 130175.
36 H. Zhang, Y. Han, J. Lai, J. Wolf, Z. Lei, Y. Yang and F. Shi, *Nat. Commun.*, 2024, **15**, 5066.
37 S. H. Han, D. Sagzhanov, J. H. Pan, B. V. Hassas, M. Rezaee, H. Akbari and R. Mensah-Biney, *ACS Sustain. Chem. Eng.*, 2022, **10**, 13495–13504.
38 L. E. Dee, P. J. Ferraro, C. N. Severen, K. A. Kimmel, E. T. Borer, J. E. K. Byrnes, A. T. Clark, Y. Hautier, A. Hector, X. Raynaud, P. B. Reich, A. J. Wright, C. A. Arnillas, K. F. Davies, A. MacDougall, A. S. Mori, M. D. Smith, P. B. Adler, J. D. Bakker, K. A. Brauman, J. Cowles, K. Komatsu, J. M. H. Knops, R. L. McCulley, J. L. Moore, J. W. Morgan, T. Ohlert, S. A. Power, L. L. Sullivan, C. Stevens and M. Loreau, *Nat. Commun.*, 2023, **14**, 2607.
39 T. Y. Mou, H. S. Pillai, S. W. Wang, M. Y. Wan, X. Han, N. M. Schweitzer, F. L. Che and H. L. Xin, *Nat. Catal.*, 2023, **6**, 122–136.
40 A. Hojjati-Najafabadi, P. N. Esfahani, F. Davar, T. M. Aminabhavi and Y. Vasseghian, *Chem. Eng. J.*, 2023, **471**, 144485.
41 Y. A. Pan, J. L. Du, J. Chen, C. Lian, S. Lin and J. G. Yu, *Desalination*, 2022, **539**, 115966.
42 J. Chen, H. F. Yuan, J. G. Yu, M. Yan, Y. Yang and S. Lin, *J. Colloid Interface Sci.*, 2023, **649**, 694–702.
43 S. K. Lv, Y. L. Zhao, L. J. Zhang, T. T. Zhang, G. F. Dong, D. X. Li, S. Cheng, S. L. Ma, S. X. Song and M. Quintana, *Chem. Eng. J.*, 2023, **472**, 145026.
44 T. R. Graham, J. Z. Hu, X. Zhang, M. Dembowski, N. R. Jaegers, C. Wan, M. Bowden, A. S. Lipton, A. R. Felmy, S. B. Clark, K. M. Rosso and C. I. Pearce, *Inorg. Chem.*, 2019, **58**, 12385–12394.
45 X. Wang and Q. Ge, *Heliyon*, 2018, **4**, e01029.